

## Evaluation of Corrosion Inhibition of Two Schiff Bases Self-Assembled Films on Carbon Steel in 0.5 M HCl

Le Ruan<sup>1</sup>, Zhe Zhang<sup>1,\*</sup>, Xiaodong Huang<sup>1</sup>, Yuzeng Lyu<sup>2</sup>, Yuqing Wen<sup>1</sup>, Wei Shang<sup>1</sup>, Ling Wu<sup>3</sup>

<sup>1</sup> Guangxi Key Laboratory of Electrochemical and Magneto-chemical Functional Materials, College of Chemistry and Bioengineering, Guilin University of Technology, Guilin 541004, PR China

<sup>2</sup> Engineering Research Center of Exploration for hidden Nonferrous and Precious Metal Ore Deposits, Ministry of Education, Guilin 541004, PR China

<sup>3</sup> School of Chemistry and Chemical Engineering, Shandong University, Jinan 250100, PR China

\*E-mail: [zhangzhe@glut.edu.cn](mailto:zhangzhe@glut.edu.cn)

Received: 18 July 2016 / Accepted: 8 November 2016 / Published: 12 December 2016

---

The corrosion behavior of aromatic aldehyde Schiff bases self-assembled (SA) films on carbon steel (CS) surface was measured by electrochemical impedance spectroscopy (EIS) and polarization curves with different immersion time. The results showed that after assembling in two Schiff base solutions for 12 h, the corrosion efficiency of the SA films on CS surface reached 92.80% and 93.66%, respectively. Scanning electron microscopy (SEM) micrographs showed that the SA films can prevent CS corrosion in HCl solution. The quantum chemical calculations and dynamic simulations were employed for investigation of the inhibition mechanism.

---

**Keywords:** corrosion; self-assembled films; carbon steel; SEM

### 1. INTRODUCTION

Iron alloys find extensive structural applications in industrial and engineering construction as materials for reaction vessels, tunnels, etc., so the corrosion of iron alloys receives a considerable amount of attention [1, 2]. Carbon steel is a common constructional material for many industrial units because of the low cost and excellent mechanical properties [3, 4]. Acid solutions are widely used in many industrial processes such as acid pickling, acid descaling and oil-well acidizing [5, 6]. However, CS is very prone to corrosion in aggressive acid solution [7, 8].

The self-assembled films is a reliable method for preparing chemically and structurally well-defined surfaces on metal surfaces which can limited the oxidation of metal [9-11]. It has been reported that the SA films of organic compounds having S, N, P, O donor sites, unsaturated bonds along with

planar conjugated aromatic moieties can form SA films which can limit the oxidation of different kinds of metals [12-15]. The advantages of SA films include simplicity of preparation, stability, ease of manipulation and the ability of different chemical functionalities at high molecular dimensions [16, 17].

Due to the presence of the  $-C=N-$  group in the molecule, Schiff bases exhibit effective corrosion inhibition for different metals and alloys [18-21]. Lashgari Et al. studied the inhibitory action of N,N'-1,3-propylen-bis (3-methoxysalicylideneimine) {PMSI} on mild steel corrosion in sulfuric acid through electrochemical methods and scanning electron micrographs, and the studies revealed that the PMSI compound is a good mixed-type inhibitor [22]. Wang et al. synthesized a series of Schiff base surfactants and evaluated the corrosion inhibition effect of the Schiff bases. Electrochemical impedance spectroscopy, polarization curves and weight loss experiments showed that the surfactant molecules were well absorbed on the CS surface and could be described using Langmuir adsorption isotherm [23].

The aim of this study is to gain some insight into the corrosion inhibition of two Schiff base compounds SA films on CS in 0.5 M HCl solution using chemical and electrochemical techniques. SEM was used to characterize the CS surface. Finally, the inhibition mechanism was interpreted using quantum chemical calculations and molecular dynamics simulations.

## 2. EXPERIMENTAL DETAILS

### 2.1. Chemicals and preparation of the SA films on CS electrode

All chemical used are analytical grade purchased from Aladdin Industrial Corporation. The chemical structures and abbreviations of 2-((1*H*-1,2,4-triazol-3-ylimino)methyl)-6-methoxyphenol (SB1) and 2-((1*H*-1,2,4-triazol-3-ylimino)methyl)-6-ethoxyphenol (SB2) are shown in Fig.1. They were synthesized from 3-amino-1,2,4-triazole, 3-methoxysalicylaldehyd and 3-ethoxysalicylaldehyde [24]. 0.005 M self-assembly solutions of two Schiff bases were obtained through dissolving relevant chemicals into the ethanol solution, and the aggressive environment used was 0.5 M HCl solution prepared from analytical reagent grade chemicals and doubly distilled water.

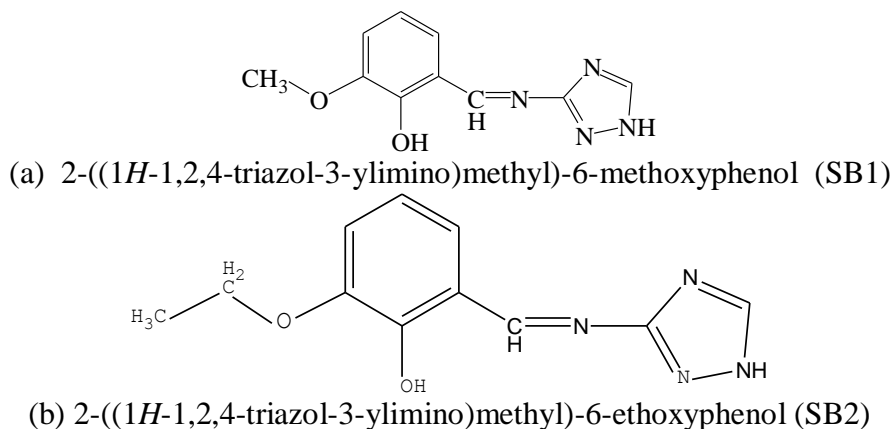


**Figure 1.** Chemical structures and abbreviation of two Schiff bases

A rod of CS (4 mm diameter) was used as working electrode, and the composition (wt%) of CS was C (0.45%), Si (0.17%), Mn (0.5%), S (0.035%), P (0.035%), Cr (0.25%), Cu (0.25%), Ni (0.30%),

Fe (the remaining 98%). The preparation and preliminary process of CS electrode referenced from the published article of Zhang et al [25, 26]. Before each test, the electrode surfaces were abraded with emery papers, and cleaned in ethanol. Then, the polished CS electrodes were immersed in the self-assembly solution of SB1 and SB2 for 2 h, 4 h, 6 h, 8 h, 10 h and 12 h.

## 2.2. Electrochemical measurements

All experiments were performed using the traditional three-compartment glass cell. The reference was a saturated calomel electrode (SCE) and the counter electrode is a Pt electrode. The EIS measurements were carried out at open circuit potential over a frequency range from 100 kHz to 0.1 Hz with sinusoidal potential perturbation 5 mV in amplitude by using a electrochemical workstation (CHI760E CH Instruments), and the EIS data were fitted using the ZView 2 software. Polarization curves of the CS electrodes covered with and without SA films were recorded by scanning speed of 2 mV/s started from -200 to +200 mV with respect to the open circuit potential versus corrosion potential. All of the experiments were conducted at  $25 \pm 1$  °C.

## 2.3. Scanning electron microscopy (SEM)

Specimen for SEM experiments were CS sheets (3 mm × 3 mm × 1 mm) corroded in 0.5 M HCl solution for 2 h with and without SA films made by immersion in SB1 and SB2 self-assembly solutions for 12 h. The surface characteristics of CS specimens were examined by JSM-6380LV SEM.

## 2.4. Quantum chemical calculation and molecular dynamic simulation

The geometries of two Schiff bases were fully optimized by the Gaussian 03 software package [27] employing the B2LYP/6-311G\* method [28]. Density functional theory (DFT) methods were used because they can reach an exactitude similar to other methods in less time and with a smaller investment from the computational point of view. The energy of the highest occupied molecular orbital ( $E_{\text{HOMO}}$ ), the energy of the lowest unoccupied molecular orbital ( $E_{\text{LUMO}}$ ),  $\Delta E = E_{\text{LUMO}} - E_{\text{HOMO}}$  and the dipole moment ( $\mu$ ) were used to analyze the inhibition capability.

In order to investigate the adsorption configuration and adsorption strength of the SA molecules on the iron surface, molecular dynamic simulations were performed using the Discover module of the Materials Studio 6.0 software developed by Accelrys Inc. [29]. The adsorption system was consisted of 400 H<sub>2</sub>O molecules, 4 H<sub>3</sub>O<sup>+</sup> ions, 4 Cl<sup>-</sup> ions and 1 inhibitor molecule. A Fe (110) surface (24.824 Å × 24.824 Å × 18.242 Å) was selected and cleaved from the Fe cell and then the surface was optimized to the energy minimum. The Fe crystal contained 10 layers total 2500 Fe atoms, then adding a vacuum layer to build up the metal surface. H<sub>2</sub>O, H<sub>3</sub>O<sup>+</sup> and Cl<sup>-</sup> units were optimized and optimized Schiff base molecules were induced. The solution layer was constructed by building solution layer and solvent layer through Modules/Amorphous/Construction. Finally, the complete simulation system was combined by Build Layer. The simulation box was 24.8238 Å × 24.8238 Å × 48.9948 Å with periodic

boundary conditions. The parameters of optimization and molecular dynamics simulation are shown in table 1.

**Table 1.** The based group Settings of molecular dynamics simulation

Basic setup	<u>Method</u>	<u>Convergence Level</u>	<u>Maximum iteration</u>	
	smart minimizer	ultra-fine	20000	
Minimizer setup	<u>forcefield</u>	<u>non-nond</u>	<u>Summation method</u>	<u>Cutoff distance</u>
	comoass	vdW	Atom based	9.5 Å
Dynamic simulation setup	<u>Ensemble</u>	<u>Thermostat</u>	<u>Simulation temperature</u>	<u>Energy deviation</u>
	NVT	Andersen	298.0 K	5000.0 kcal/mol
	<u>Dynamics time</u>	<u>Time step</u>	<u>Frame output</u>	
	2000.0ps	1 fs	Every 1000 steps	

### 3. RESULTS AND DISCUSSION

#### 3.1. EIS measurements

SA films of SB1 and SB2 prepared on the CS surface were investigated by EIS. Fig. 2 shows the Nyquist plots in 0.5 M HCl solution for the bare CS electrode and SA films modified CS electrodes by immersion in the assembly solution from 2h to 12h. It can be seen from Fig. 1 that the Nyquist plots of CS electrode does not yield perfect semicircle as expected from the theory of EIS, which is caused by surface roughness and is known as the “dispersing effect” [30]. The slightly depressed semicircle indicates that the corrosion of CS in 0.5 M HCl solution is mainly controlled by transfer process [31, 32]. The diameter of semicircle increases after the modification with Schiff base SA films on the CS surface. This increase is more pronounced with increasing immersion time which indicates adsorption of Schiff base molecules on the CS surface. All the EIS data are fitted with the equivalent circuit (Fig. 2) which is a parallel combination of the charge transfer resistance ( $R_{ct}$ ) and the constant phase element (CPE), both in series with the solution resistance ( $R_s$ ). The impedance function of a CPE is defined by the mathematical expression given below :

$$Y_{CPE} = Y_0(j\omega)^{-n} \quad (1)$$

$$Z_{CPE} = \frac{1}{Y_0}(j\omega)^n \quad (2)$$

where  $Y_0$  is modulus,  $j$  is the imaginary root,  $\omega$  is the angular frequency and  $n$  is the phase. The calculated inhibition efficiency,  $\eta\%$  is calculated from the following equation:

$$\eta_R = \frac{R_{ct} - R_{ct}^0}{R_{ct}} \times 100\% \quad (3)$$

where  $R_{ct}$  and  $R_{ct}^0$  are the charge transfer resistance values with and without SA films on carbon steel surface, respectively. The values of CPE capacitance ( $C_{dl}$ ) are calculated using Eq. (4):

$$C_{dl} = \frac{\epsilon_0 \epsilon S}{d} \tag{4}$$

where  $\epsilon_0$  is the permittivity of air,  $\epsilon$  is the local dielectric constant,  $d$  is the film thickness and  $S$  is the electrode surface. The measured impedance data analyzed with ZView2 software for the equivalent circuit and the calculated  $\eta$  are shown in Table 2.

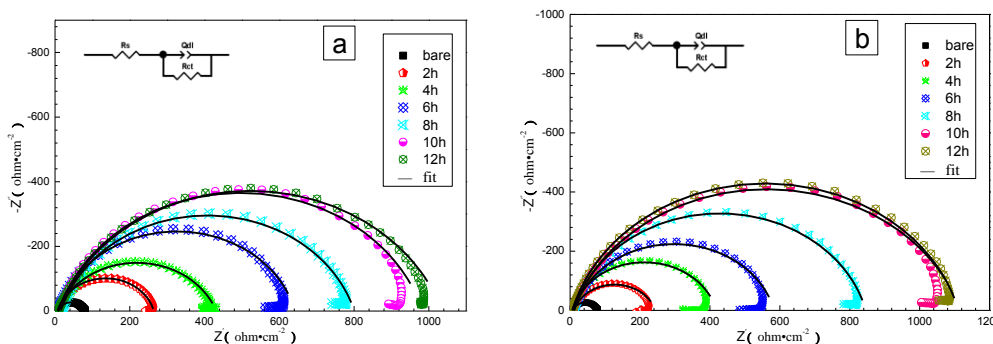


**Figure 2.** Nyquist impedance spectra of the bare working electrode and the working electrode covered with SA films with a long immersion time in SB2 (a) and SB1 (b). The solid lines are their fitted curves

**Table 2.** Element value of a circuit equivalent to fit the impedance spectra in Fig. 2 and the values of the corrosion efficiency ( $\eta$ ) calculated by Eq. (3).

Self-assembly molecules	time (h)	$R_s$ ( $\Omega\text{cm}^2$ )	$R_{ct}$ ( $\Omega\text{cm}^2$ )	CPE		$C_{dl}$ ( $\mu\text{F cm}^{-2}$ )	$\eta$ (%)	
				$n$ (0-1)	$Y_0(\mu\Omega^{-1}\text{s}^n\text{cm}^{-2})$			
bare	0	8.32	69.94	0.84	44.26	14.226	—	
	2	6.71	257.8	0.84	13.85	4.24	72.87	
	4	8.94	398.5	0.84	13.39	4.42	82.45	
	SB1	6	7.10	424.5	0.78	18.90	12.46	83.52
		8	9.35	626.3	0.84	11.50	4.02	88.83
		10	3.80	788.1	0.82	11.60	5.18	91.13
12		9.70	971.4	0.82	15.90	7.97	92.80	
SB2	2	10.16	230.9	0.82	20.47	13.11	69.71	
	4	6.57	407.3	0.85	12.38	5.57	82.83	
	6	11.73	572.1	0.84	9.96	5.17	87.77	
	8	10.77	835.2	0.85	9.11	4.41	91.63	
	10	6.38	1107.0	0.84	8.96	5.17	93.68	
	12	7.86	1104.0	0.81	1.43	1.38	93.66	

It can be seen from Table 2, the  $R_{ct}$  increases with the assembly time and the  $C_{dl}$  value decreases with the immersion time. This might be due to the substitute of  $\text{H}_2\text{O}$  molecules by Schiff bases molecules

with small dielectric constant. The adsorption Schiff base molecules increase the thickness of the double layer capacitance which can increase the  $R_{ct}$  and decrease the corrosion reaction rate. After immersion in self-assembly solution for 12 h, the corrosion inhibition of SB1 and SB2 SA films on CS surface reach 92.80% and 93.66%, respectively. Both of the Schiff bases contain benzene ring and -C=N- group that can be the adsorption center to form SA films on CS surface. At short Schiff compounds assembling time, the molecules are loosely arranged on the CS surface. When the assembling time reaches 8 hours, the SA films are well organized [33]. The EIS result has the similar conclusion with the research of Issaadi et al [34] using the novel thiophene symmetrical Schiff base compounds as corrosion inhibitor for mild steel. The Schiff compound adsorption on the metal surface lead to the formation of a surface film in the acidic solution can increase the  $R_{ct}$  and protect the metal from corrosive attack.

### 3.2. Polarization curves

Fig. 3 shows the potentiodynamic polarization curves of CS covered with and without Schiff bases SA films in 0.5 M HCl. Both the cathodic current and the anodic current decrease in the presence of the SA films on CS surface, which means that the Schiff base molecules are adsorbed on the CS surface and block the reaction sites of the CS surface. The maximum displacement in  $E_{corr}$  value in present study is 24 mV, which indicates that the two Schiff bases are mixed-type inhibitor [35]. The values of corrosion current ( $I_{corr}$ ), corrosion potential ( $E_{corr}$ ), cathodic and anodic Tafel slopes obtained by the anodic and cathodic regions of the Tafel plots are shown in Table 3. The corrosion current density is calculated from the extrapolation of straight part of the Tafel lines and the inhibition efficiency ( $\eta\%$ ) values are calculated from Eq. (5):

$$\eta = \frac{i_{corr}^0 - i_{corr}}{i_{corr}^0} \times 100\% \quad (5)$$

From Table 3, it can be seen that the corrosion rate decreased and the corrosion efficiency increase with the immersion time. Both anodic metal dissolution of iron and cathodic hydrogen evolution reactions are inhibited after the formation of Schiff compound SA films on CS surface. The shift in corrosion potential is very slight compared with the corrosion potential observed in blank solution so that the two Schiff compounds can be classified as mixed type corrosion inhibitor [36, 37]. When the immersion time reaches 12 h, the  $\eta$  of SA films on CS surface reaches 92.99% and 94.68%, respectively, which gives the same efficiency trend as found in EIS measurements.

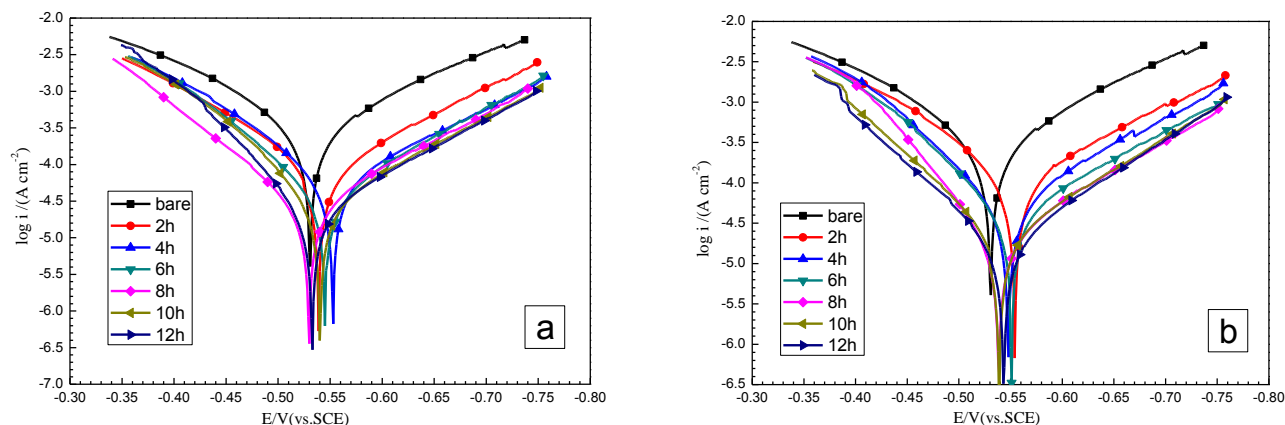


**Figure 3.** Polarization parameters of the bare CS electrode and the CS electrodes covered with SA films measured in HCl solution with prolonged immersion time in SB1 (a) and SB2 (b) solutions

**Table 3.** Polarization parameters for the bare CS electrode and the CS electrodes covered with SA films in 0.5 M HCl solution

Assembly molecule	Assembly time (h)	$E_{corr}$ (V vs .SCE)	$-\beta_c$ (V dec <sup>-1</sup> )	$\beta_a$ (V dec <sup>-1</sup> )	$i_{corr}$ ( $\mu\text{Acm}^{-2}$ )	$\eta$ (%)
bare	0	-0.531	0.149	0.129	310.4	—
	2	-0.539	0.149	0.121	90.088	70.98
	4	-0.553	0.146	0.101	65.38	78.94
	6	-0.54	0.128	0.088	42.86	86.19
	8	-0.531	0.135	0.091	28.16	90.93
	10	-0.541	0.130	0.075	29.2	90.59
	12	-0.532	0.129	0.071	21.75	92.99
SB1	2	-0.555	0.162	0.117	126.9	59.12
	4	-0.548	0.129	0.089	54.3	82.51
	6	-0.55	0.140	0.087	47.67	84.64
	8	-0.539	0.135	0.072	20.19	93.50
	10	-0.539	0.130	0.086	23.82	92.33
	12	-0.544	0.122	0.071	16.5	94.68

### 3.3. Surface analysis studies

Fig. 4 represents the SEM images of the CS samples modified without and with Schiff bases SA films after corroded in HCl solution for 2 h. Fig. 1a is the image of the CS sheets corroded in HCl for 2 h and it can obviously be seen that the surface of CS sample is strong damaged. Fig. 3b shows the image of the SB1 modified CS surface. The CS surface is damaged after 2 h corroded in HCl, but its surface looks better than the CS surface without SA film. As can be seen from Fig.3c, the SB2 modified CS surface is less damaged, which confirms the inhibition effect. Therefore, it can be concluded that both

of the two Schiff bases have good inhibiting ability for CS corrosion and SB2 SA films has better inhibiting action on CS surface.

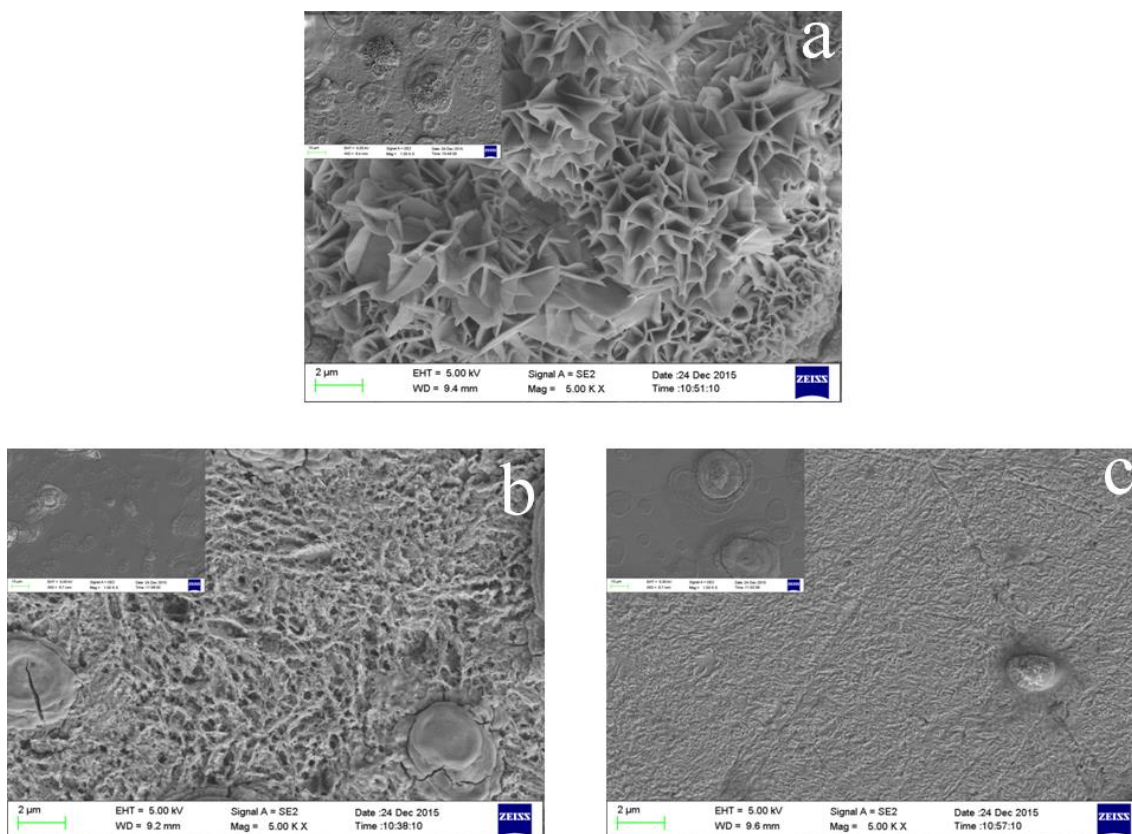


**Figure 4.** SEM images obtained from CS sheets without and with SA films in 0.5 M HCl for 2 h: (a) bare, (b) SB1, (c) SB2

### 3.4. Quantum chemical calculation and molecular dynamic simulation

#### 3.4.1 Quantum chemical calculation

Quantum chemical calculation were carried out to find the relationship between the Schiff base molecule structure and its inhibition effect. Fig. 5 is the  $E_{\text{HOMO}}$  (highest occupied molecular orbital) energy and  $E_{\text{LUMO}}$  (lowest unoccupied molecular orbital) energy calculated at B2LY/6-311\* level and the quantum chemical parameters are shown in Table 4. It has been found that the HOMO is located in the region around the  $-\text{C}=\text{N}-$  group and benzene ring. This probably indicates that the preferred active sites for an electronic attack and the favorite sites to interact with the CS surface are located within the region around N atom and benzene ring.

The LUMO of TA is distributed all over the molecule and the LUMO of the three Schiff bases is distributed over the inhibitor molecule except for hydrogen atoms. It can be concluded the unoccupied d orbit of Fe can both form coordinate bond with HOMO orbit and form back-donation bond with LUMO orbit. So the Schiff base molecules are in combination with carbon steel surface with chemical bond

which prevent the carbon steel from corrosion in the erosive solution. It is well known that the  $E_{\text{HOMO}}$  is associated with the electron donating ability of a molecule and the  $E_{\text{LUMO}}$  indicates the ability of the molecules to accept electrons. High  $E_{\text{HOMO}}$  value is likely to indicate a tendency of the molecule to donate electrons to appropriate acceptors with low energy and empty molecular orbital, and low  $E_{\text{LUMO}}$  means the high accept electrons ability.

**Table 4.** Quantum chemical parameters calculated using the B3LYP method with a 6-311G (d, p) basis set for inhibitors molecules

Assembly molecule	$E_{\text{HOMO}}$ (eV)	$E_{\text{LUMO}}$ (eV)	$\Delta E$ (eV)	$\mu$ (Debye)	$\chi = (I+A)/2$	$\gamma = (I-A)/2$	$\Delta N_{\text{Fe}}$	$\eta_{10\text{h}}$ (%)
SB1	-5.92	-1.61	4.31	3.40	3.77	2.15	0.75	92.99
SB2	-5.89	-1.59	4.30	3.40	3.74	2.15	0.76	94.68

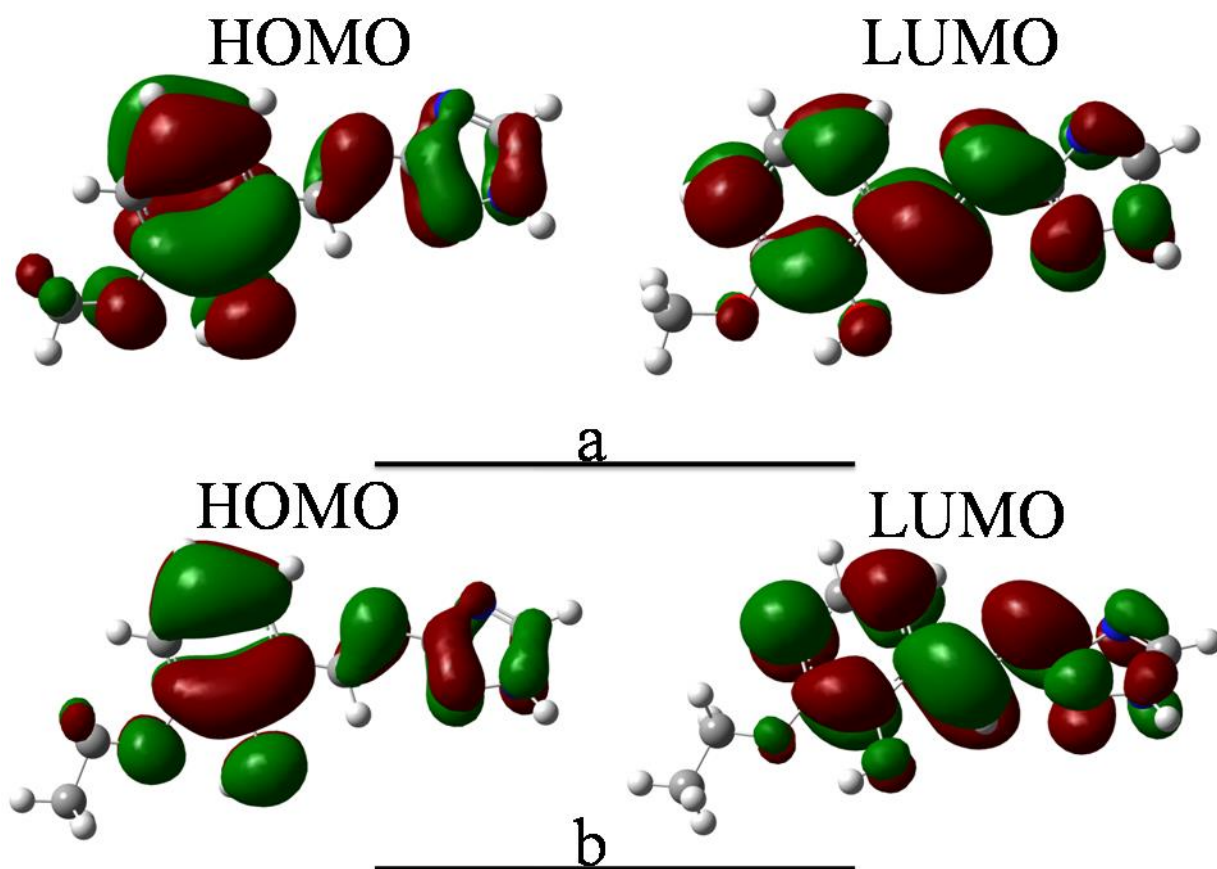


**Figure 5.** The HOMO and LUMO molecular orbitals of self-assembly molecule: SB1 (a) SB2 (b)

The energies of  $E_{\text{HOMO}}$  and  $E_{\text{LUMO}}$  are related to the ionization potential ( $I$ ) and the electron affinity ( $A$ ) of the iron atoms and the inhibitor molecules, defined as  $I = -E_{\text{HOMO}}$  and  $A = -E_{\text{LUMO}}$ . The

absolute electronegativity( $\chi$ ) and the global hardness ( $\gamma$ ) of the inhibitor molecule are approximated by Eqs. (6) and (7):

$$\chi = \frac{I + A}{2} \quad (6)$$

$$\gamma = \frac{I - A}{2} \quad (7)$$

Thus, the fraction of electrons transferred from the inhibitor to metallic surface ( $\Delta N$ ) is calculated by Eq. (8) [38]:

$$\Delta N = \frac{\chi_{\text{Fe}} - \chi_{\text{inh}}}{2(\gamma_{\text{Fe}} + \gamma_{\text{inh}})} \quad (8)$$

where the  $\chi_{\text{Fe}}$  and  $\gamma_{\text{Fe}}$  are the absolute electronegativity and global hardness of the Fe atom, and the  $\chi_{\text{inh}}$  and  $\gamma_{\text{inh}}$  are the absolute electronegativity and global hardness of the self-assembled molecules. The theoretical values of  $\chi_{\text{Fe}}$  and  $\gamma_{\text{Fe}}$  are 7 eV and 0 eV [39]. According to Lukovits, if  $\Delta N < 3.6$ , the inhibition efficiency increases with increasing electron-donating ability at the metal surface [40]. The  $\Delta N$  values for SB1 and SB2 are all less than 3.6, which means that the increase in inhibition efficiency is due solely to the electron donating ability of the inhibitor. Agreeing with Ju study [41], SB2 has the higher inhibition efficiency because it has higher HOMO energy and  $\Delta N$  values, and it has better ability of offering electrons.

### 3.4.2. Molecular dynamic simulation

Molecular dynamic simulation was used to further investigate the adsorption behavior of SB1 and SB2 molecules on the Fe (110) surface by Discover module of Material Studio 6.0 software. The adsorption intensity of the SA molecules can be evaluated with the binding energy ( $E_{\text{binding}}$ ), which can be calculated by Eqn (9) and (10):

$$E_{\text{adsorption}} = E_{\text{total}} - (E_{\text{surface+solution}} + E_{\text{inhibitor+solution}}) + E_{\text{solution}} \quad (9)$$

$$E_{\text{binding}} = -E_{\text{adsorption}} \quad (10)$$

where  $E_{\text{total}}$  is the total potential energy of the system,  $E_{\text{surface+solution}}$  and  $E_{\text{inhibitor+solution}}$  are the potential energies of the system without the SA films and the system without the Fe surface, respectively.  $E_{\text{solution}}$  is the potential energy of all of the water molecules. The calculated  $E_{\text{binding}}$ ,  $E_{\text{adsorption}}$  and the inhibition efficiency of SA films are listed in table 5 and the equilibrium configuration of the simulated system are shown in Fig. 6. As seen in table 5, the values of binding energies of SB1 and SB2 are positive, indicating that both of the Schiff compounds can be adsorbed on the Fe surface [42]. The  $\pi$  electron of the hetero-cyclic ring and benzene ring of Schiff bases can combine the inhibitor molecules with Fe atoms by covalent bonds. The Schiff base molecules can combine with the iron atoms by forming covalent bonds through the  $\pi$  electron of hetero-cyclic ring and benzene ring of Schiff bases with the unsaturated orbital of  $\text{Fe}3d^64s^2$ . The Schiff base molecules adsorbed on the iron surface have a planar structure through the absorption center of benzene ring and triazole ring. The higher binding energy value of SB2 suggests a stable and better adsorption profile for SB2 with comparatively higher inhibition

efficiency. It is due to the ethoxy has stronger supplying electron ability, so the SB2 molecules can be more easily absorbed on iron surface than SB1 molecules and have higher inhibition efficiency.

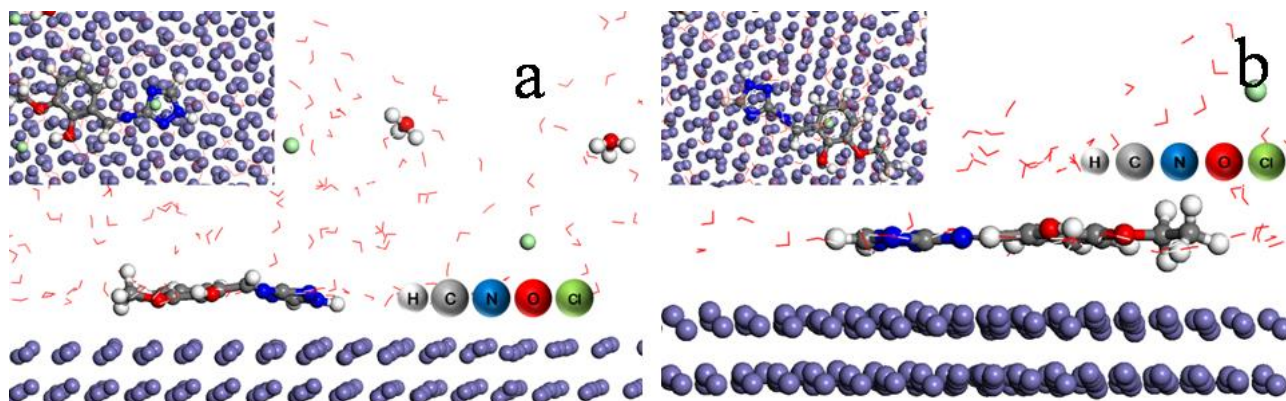


**Figure 6.** Equilibrium adsorption configuration of self-assembly molecules: SB1 (a), SB2 (b)

**Table 5.** Interaction and binding energy of the SB1 and SB2 on Fe (1 1 0) surface

Assembly molecule	$E_{\text{adsorption}}$ (eV)	$E_{\text{binding}}$ (eV)	$\eta_{12\text{h}}$ (%)
SB1	-4.246	2.246	92.80
SB2	-4.288	4.288	93.66

#### 4. CONCLUSIONS

Two Schiff bases self-assembled films were formed on CS surface and investigated in 0.5 M HCl solution for different immersion time using a series of techniques. EIS measurements shows that SB1 and SB2 SA films have excellent inhibition effect for the corrosion of CS in 0.5 M HCl solution. The inhibition efficiency of the SA films on CS surface increases with the immersion time. The potentiodynamic polarization curves indicate that the Schiff bases SA films behave as mixed-type corrosion inhibitor by inhibiting both anodic iron dissolution and cathodic hydrogen evolution reactions. SEM images, Quantum chemical calculation and molecular dynamic simulation confirm that SB1 and SB2 can absorb on CS surface and inhibit the corrosion of iron.

#### ACKNOWLEDGEMENTS

This work was funded by Guangxi Natural Science Foundation (No. 2016GXNSFJJA120133), the key project of science and technology research in universities of Guangxi (2013ZD029).

**References**

1. E. E. Oguzie, C. K. Enenebeaku, C. O. Akalezi, S. C. Okoro, A. A. Ayuk, E. N. Ejike, *J Colloid Interf Sci.*, 349 (2010) 283-292.
2. N. D. Nam, Q. V. Bui, M. Mathesh, M. Y. J. Tan, M. Forsyth, *Corros. Sci.*, 76 (2013) 257-266.
3. H. A. El-Lateef, V. M. Abbasov, L. I. Aliyeva, E. E. Qasimov, I. T. Ismayilov, *Mater. Chem. phys.*, 142 (2013) 502-512 .
4. F. E. Heakal, A. S. Fouda, S. S. Zahran, *Int. J. Electrochem. Sci.*, 10 (2015) 1595-1615.
5. M. Belkhaouda, L. Bammou, R. Salghi, A. Zarrouk, E.E. Ebenso, H. Zarrok, B. Hammouti, *Int. J. Electrochem. Sci.*, 8 (2013) 10987- 10999.
6. S. Sathiyarayanan, C. Marikkannu, N. Palaniswamy, *Appl. Surf. Sci.*, 241 (2005) 477-484.
7. I. Ahamad, R. Prasad, M.A. Quraishi, *Corros. Sci.*, 52 (2010) 1472-1481.
8. A. K. Singh, M.A. Quraishi, *Corros. Sci.*, 52 (2010) 152-160.
9. F. Yu, S. Chen, H. Li, L. Yang, Y. Yin, *Thin Solid Films*, 520 (2012) 4990-4995.
10. A. Mahapatro, D. M. Johnson, D. N. Patel, M. D. Feldman, A. A. Ayon, C. M. Agrawal, *Langmuir*, 22 (2006) 901-905.
11. D. Zhang, X. He, Q. Cai, L. Gao, G. Kim, *Thin Solid Films*, 518 (2010) 2745-2749.
12. B. B. A. Rao, M. N. Reddy, *J. Chem. Sci.*, 125 (2013) 1325-1338.
13. L. Qiao, Y. Wang, W. Wang, M. Mohedano, C. Gong, J. Gao, *Mater. Trans.*, 55 (2014) 1337-1343.
14. A. O. W. Neto, E. F. Moura, H. S. Jnior, T. N. C. Dantas, A. A. D Neto, A. Gurgel, *Colloids Surf.*, A 398 (2012) 76-83.
15. M. Maxisch, P. Thissen, M. Giza, G. Grundmeier, *Langmuir*, 27 (2011) 6042-6048.
16. S. Flink, B. A. Boukamp, A. Van den Berg, F. C. J. M. Van Veggel, D. N. Reinhoudt, *J. Am. Chem. Soc.*, 120 (1998) 4652-4657.
17. G. Rajkumar, M. G. Sethuraman, *Res, Chem, Intermed.*, 42 (2016) 1809-1821.
18. S. Thirugnanaselvi, S. Kuttirani, A. R. Emelda, *Trans. Nonferrous Met. Soc. China* 24 (2014) 1969-1977.
19. Y. Zhou, S. Zhang, L. Guo, S. Xu, H. Lu, F. Gao, *Int. J. Electrochem. Sci.*, 10 (2015) 2072 – 2087.
20. A. Aytac, S. Bilgic, G. Gece, N. Ancin, S. G. Öztas, *Mater Corros.*, 63 (2012) 729-734.
21. D. Seifzadeh, H. Basharnavaz, A. Bezaatpour, *Mater. Chem. Phys.*, 138 (2013) 794-802.
22. M. Lashgari, M. R. Arshadi, S. Miandari, *Electrochim. Acta.*, 55 (2010) 6058-6063.
23. C. Wang, Y. Li, W. Zhou, *Int. J. Electrochem. Sci.*, 11 (2016) 4399-4409.
24. K. M. Khan, S. Siddiqui, M. Saleem, M. Taha, S. M. Saad, S. Perveen, M. I. Choudhary, *Bioorgan. Med. Chem.*, 22 (2014) 6509-6514.
25. Z. Zhang, N. Tian, L. Zhang, L. Wu, *Corros. Sci.*, 98 (2015) 438-449.
26. Z. Zhang, N. Tian, X. Huang, W. Shang, L. Wu, *RSC Adv.*, 6 (2016) 22250-22268.
27. M. J. Frisch, G. W. Trucks, H. B. Schlegel, G. E. Scuseria, M. A. Robb, J. R. Cheeseman, J. A. Montgomery, Jr., T. Vreven, K. N. Kudin, J. C. Burant, J. M. Millam, S. S. Iyengar, J. Tomasi, V. Barone, B. Mennucci, M. Cossi, G. Scalmani, N. Rega, G. A. Petersson, H. Nakatsuji, M. Hada, M. Ehara, K. Toyota, R. Fukuda, J. Hasegawa, M. Ishida, T. Nakajima, Y. Honda, O. Kitao, H. Nakai, M. Klene, X. Li, J. E. Knox, H. P. Hratchian, J. B. Cross, C. Adamo, J. Jaramillo, R. Gomperts, R. E. Stratmann, O. Yazyev, A. J. Austin, R. Cammi, C. Pomelli, J. W. Ochterski, P. Y. Ayala, K. Morokuma, G. A. Voth, P. Salvador, J. J. Dannenberg, V. G. Zakrzewski, S. Dapprich, A. D. Daniels, M. C. Strain, O. Farkas, D. K. Malick, A. D. Rabuck, K. Raghavachari, J. B. Foresman, J. V. Ortiz, Q. Cui, A. G. Baboul, S. Clifford, J. Cioslowski, B. B. Stefanov, G. Liu, A. Liashenko, P. Piskorz, I. Komaromi, R. L. Martin, D. J. Fox, T. Keith, M. A. Al-Laham, C. Y. Peng, A. Nanayakkara, M. Challacombe, P. M. W. Gill, B. Johnson, W. Chen, M. W. Wong, C. Gonzalez, and J. A. Pople, Gaussian, Inc., Wallingford CT, 2004.
28. A.D. Becke, *Phys. Rev. A* 38 (1988) 3098-3100.
29. Materials Studio, Revision 6.0, Accelrys Inc., San Diego, USA, 2011

30. E. Mccafferty, *Corros. Sci.*, 39 (1997) 243-254.
31. F. Touhami, A. Aouniti, Y. Abed, B. Hammouti, S. Kertit, A. Ramdani, K. Elkacemi, *Corros. Sci.*, 42 (2000) 929–940.
32. R. Solmaz, *Corros. Sci.*, 52 (2010) 3321-3330.
33. Z. Li, L. Jin, W. Wang, S. Wan, *Int. J. Electrochem. Sci.*, 8 (2013) 6513-6523.
34. S. Issaadi, T. Douadi, A. Zouaoui, S. Chafaa, M. A. Khan, G. Bouet, *Corros. Sci.*, 53 (2011)1494-1488.
35. M. Behpour, N. Mohammadi, *Corros. Sci.*, 65 (2012) 331-339.
36. R. Solmaz. *Corros. Sci.*, 52(2012) 3321-3330.
37. M. Abdallah. B. H. Asghar. I. Zaafarany, A. S. Fouda, *Int. J. Electrochem. Sci.*, 7 (2012) 282-304.
38. H. Zhao, X. Zhang, L. Ji, H. Hu, Q. Li, *Corros. Sci.*, 83 (2014) 261.
39. A. Kokalj, *Chem. Phys.*, 393 (2012)1-12.
40. H. Ju, Z. P. Kai, Y. Li, *Corros. Sci.*,50 (2008)865-871.
41. H. Ju, Z. P. Kai, Y. Li, *Corros. Sci.*, 50(2008) 865-871.
42. L. Li, X. Zhang, S. Gong, H. Zhao, Y. Bai, Q. Li, L. Ji, *Corros. Sci.*, 99 (2015) 76-88

© 2017 The Authors. Published by ESG ([www.electrochemsci.org](http://www.electrochemsci.org)). This article is an open access article distributed under the terms and conditions of the Creative Commons Attribution license (<http://creativecommons.org/licenses/by/4.0/>).